Cusp Slope Limit Analysis of Double Image Gravitational Lenses

© **P. T. Mutka** [1,2]

[1] University of Oulu, Oulu, Finland
[2] Email: petri.mutka@oulu.fi

Abstract: We have developed an analytical theory for axially symmetric lensing with generalized mass density profile [1]. We apply the theory to the statistical study of double-image quasar lenses. Our aim is to recover a universal cusp slope value for the dark matter halo profiles responsible for lensing. Our lensing model gives a relation between location of the optical axis, the cusp slope of the density profile and the magnification ratio of the images. It does not depend directly on cosmology, distance of the lens, distance of the source nor mass of the lens object. We use this relation to derive statistics of the upper limits for the cusp slopes, which are capable producing observed magnification ratios for each lens. The composition of this distribution depends on the general properties of the dark matter halos [2].
The distortions to the statistics originate from several sources: the lens ellipticity, differential extinction, the variability of the source coupled with the time delay effects and the galactic microlensing or the microlensing by substructure within the lens. In our method these effects can be considered as a statistical noise. Magnitude of these factors will be studied by using mock data.
We present preliminary results acquired from the CSL analysis, that do not incorporate detailed error analysis. Our method suggests two lens object populations with cusp slopes $\alpha_I = -1.96$ and $\alpha_{II} = -1.49$, and corresponding occurrence probabilities $P_I = 0.83$ and $P_{II} = 0.17$.

1. Introduction

According to the current understanding, the large scale structure of the universe is generated by gravitationally collapsed non-interacting cold dark matter governed by the expansion of the Universe and cosmological constant (LCDM-model). This structure formation paradigm has been very successful at the linear regime when considering observed properties of the Universe at the large scale. At the nonlinear scale of galaxy clusters and individual galaxies, the structure formation is more strongly coupled to the physical properties of the unknown dark matter halo particles, that are not yet properly understood. Nonlinear halo formation is a very complicated problem involving galactic dynamics and kinematics, including dynamical interactions of poorly understood dark matter halos and their merging processes [3,4].

This problem becomes more tractable with increasing computing power. Massive N-body computer simulations on large scale structure formation has been conducted by several collaborations, see for example [5]. However, the resolution of these N-body simulations is not sufficient to study strongly nonlinear central regimes of the dark matter halos. This resolution problem has been tackled with a nested simulation method, producing evidence that unperturbed dark matter halos evolve towards a relaxed state with a universal density profile [6,7,8]. In spite of this, the resolution of the simulations can be questioned. Even a single galaxy provides a formidable problem for a faithful N-body modeling especially at the central regions. Although these simulations have been complemented with theoretical studies, the exact form and existence of this universal density profile is still debated [9,10]. Since the exact nature of the dark matter remains a mystery, the physical assumption of the noninteracting dark matter in the N-body simulations must be re-examined at the dense central regions of the dark matter halos.

The N-body simulation studies of dark matter halos have produced a host of different halo models with varying degrees of freedom [6,7,8,11,12,13]. All these models share some general properties. At the central region the halos are cusped following a power law, e. g. $\rho \propto r^{\alpha}$, where $\alpha < 0$. At the scale region $r \sim 1$, the exponent of the power law is changing to $\rho \propto r^{-3}$.

The models are conflicting with the observations at several areas. The gravitational lensing data and single universal density profiles can not be fully reconciliated with high resolution N-body data [14,15]. The unobserved substructure within the halos has been proposed as a culprit for anomalous flux ratios produced by some lens systems [16]. Furthermore the theory underestimates the proportion of quadrupole lenses and arcs [17]. The problems with the universal density profile culminate at the scale of individual galaxies [18]. Especially, the density profiles of dwarf galaxies and rotation curves exhibit inconsistencies [19].

Here we present results from a preliminary study. We have developed a statistical method for recovering cusp slope populations for density profiles of a double image lens system sample. The method is based on our analytical theory for axially symmetric lensing employing the GNFW profile [6,7,8]. The density profile is strongly cusped at the center, i. e. when $r \ll 1$, mass density $\rho \propto r^{\alpha}$, where $\alpha = [-2, -1)$ is a free parameter. The lensing model gives a relation between location of the optical axis, the cusp slope and the

magnification ratio of the images. It does not depend directly on the cosmology, distances of the lens and the source nor mass of the lens object. We use this relation to derive statistics of the upper limits for the cusp slopes, which are capable producing observed magnification ratios for each lens (CSL-limit). The composition of this distribution depends on the general properties of the lens dark matter halos [2]. For example, a single population of halos with a universal cusp slope shows a distinct signature in the distribution of the CSL values. We apply our method to a carefully sampled ensemble of the observed double-image quasar lenses, which resemble systems with a high degree of axial symmetry.

The resulting statistics include distortions by the lens ellipticity (or other deviations from the axial symmetry), differential extinction, the variability of the source coupled with the time delay effects and perturbations by the substructure within the lens and possibly microlensing. Magnitude of these perturbations on the overall statistics of the cusp slope limits (CSL) will be studied by creating mock lens catalogues.

Here we briefly review the central results from the lensing theory leading to the CSL formalism. Subsequently, we describe the data used in the analysis and the method for creating the mock lens catalogues. We discuss different perturbation sources for the statistics and present preliminary results from the analysis.

2. The lens equation

The lens equation produced by a GNFW halo with a cusp slope $\alpha = [-2, -1)$ becomes particularly simple when it is normalized with the Einstein radius of the lens [1]:

$$l = \begin{cases} qk(1 - |k|^{\alpha+1}) & k \leq k_B \\ k - \frac{\alpha+1}{\alpha+3}\frac{k_B^2}{k}(1-q) & k > k_B \end{cases} . \quad (1)$$

Here k is a radial coordinate at the lens plane and l corresponding coordinate at the source plane. Information on the cosmology, the lens distance, the source distance, the mass and the concentration of the lens object is embedded in the constant q. See [1] for further details. The lens equation (1) has a piecewise definition, that is divided at

$$k_B = \left(\frac{2(q-1)}{q(\alpha+3)}\right)^{1/(\alpha+1)} \quad (2)$$

in order to avoid negative surface densities.

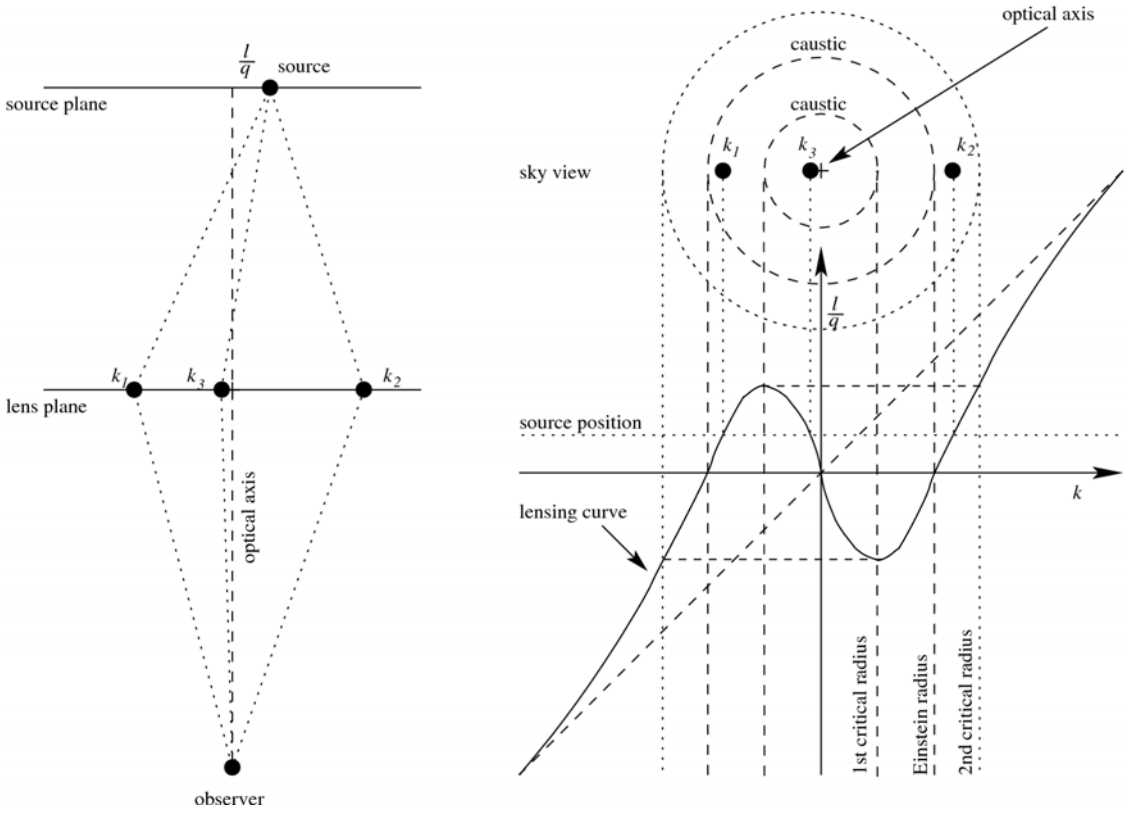

Fig. 1. Lensing geometry and the critical points at the lensing curve. The source image at the maximum offset from the optical axis produces images at the first critical radius k_{cr1} and at the second critical radius k_{cr2}.

The lens system with the source at the maximum source coordinate $l = l_{max}$ produces images at k_{cr1} and k_{cr2}. At k_{cr1} derivative of the lens equation (1) vanishes, and it can be solved as

$$k_{cr1} = (\alpha + 2)^{-1/(\alpha+1)} \tag{3}$$

Because $q > 1$ by it's definition in [1], it is easy to see that $k_B > (2/(\alpha + 3))^{1/(\alpha+1)} > k_{cr1}$ holds always. Therefore the maximum source coordinate l_{max} for strong lensing can be solved by setting $k = k_{cr1}$ in the lens equation (1), which gives

$$l_{max} = -qk_{cr1}\frac{\alpha+1}{\alpha+2} \tag{4}$$

See figure 1.

3. Observational data

For this study, we composed a catalogue of dual imaged lens systems, which resemble closely to axially symmetric lensing. The catalogue contains data from JVAS/CLASS radio survey [20] and CASTLES survey [21]. Our sample has 44 lens systems, see [2] for further details. Five of these systems had no data available during the conducted background research, which reduces number of useful systems to 39.

The included systems were chosen with the following criteria: Lens system must have two clearly separate lensed images corresponding to a lensed quasar. Triple and quad lenses and Einstein rings were excluded. Clearly non-axially-symmetric cases were also excluded from the data. Additional lensed components, such as radio jets were allowed as long as the lensed point source was present.

All the available flux measurements from optical and radio observations were used to calculate the mean flux ratio weighed with the measurement errors in the observations. The flux ratio is calculated by dividing the dimmer image flux with the brighter image flux. Thus, the ratio is always below unity. No attempt for correcting extinction or possible time-delay effects were made.

4. CSL analysis

Magnification of the images, cumulative mass function, convergence and shear of the lens can be ac-

quired from the lens equation (1) as well. In general, for strong lensing it holds

$$\frac{|k_1|^{\alpha+2}+|k_2|^{\alpha+2}}{|k_1|+|k_2|} = 1 \tag{5}$$

for the solutions of images k_1 and k_2 when $k_1, k_2 < k_B$. Equation (5) holds most of the time, and it starts to break-up only with large lens masses or concentrations when k_1 or k_2 exceeds the value k_B. With the lens equation (1) and the relation (5) the magnification ratio $M = \mu_1/\mu_2$ of the images k_1 and k_2 produced by the source at l can be written as

$$M = \frac{\mu_1}{\mu_2} = \theta \frac{|\theta^{\alpha+2}+1-(1+\theta)(\alpha+2)|}{|\theta^{\alpha+2}+1-\theta^{\alpha+1}(1+\theta)(\alpha+2)|}. \tag{6}$$

Note that constant q has vanished from this expression. It is also possible to parametrize the lens equation with coordinate ratio $\theta = k_1/k_2$.

A solution $\alpha = \alpha_{CSL}$ and $\theta = \theta_{CSL}$ for the following pair of equations

$$\begin{cases} \frac{dM}{d\theta} &= 0 \\ M &= M_0 \end{cases} \tag{7}$$

gives a CSL limit for the lens system. Here M_0 is the measured magnification ratio of the lens system. The value α_{CSL} is the minimum amount of "cuspiness", i. e. the maximum value for α, that is needed to produce the observed magnification ratio M_0 with any lensing geometry assuming the axial symmetry. Remarkable property of the CSL-value is that no information about the location of the mass center or the optical axis of the lens system is required [2].

The statistics of α_{CSL} values are constructed by assuming that the source images are uniformly distributed at the source plane within a circle bounded by $l = l_{max}$. If all the lens systems in the sample have the same universal cusp slope value, a distinctive distribution of α_{CSL} values is produced, as in figure 2. If the cusp slopes of the halos are randomly distributed in some range of values, this feature is destroyed.

The best fit for the theoretical CSL-distribution to the observed data indicates that there is a major population of lens systems with a universal cusp slope $\alpha \approx -1.95$. The data also suggests a second population of lenses with a cusp slope $\alpha = -1.49$. Roughly one out of six systems belongs to this second population of lens objects. The similar CSL-distribution is acquired from a mock data created with aforementioned population ratios and cusp slope values. See figure 2 and it's caption for further details. Acquired CSL-fits are summarized in table 1.

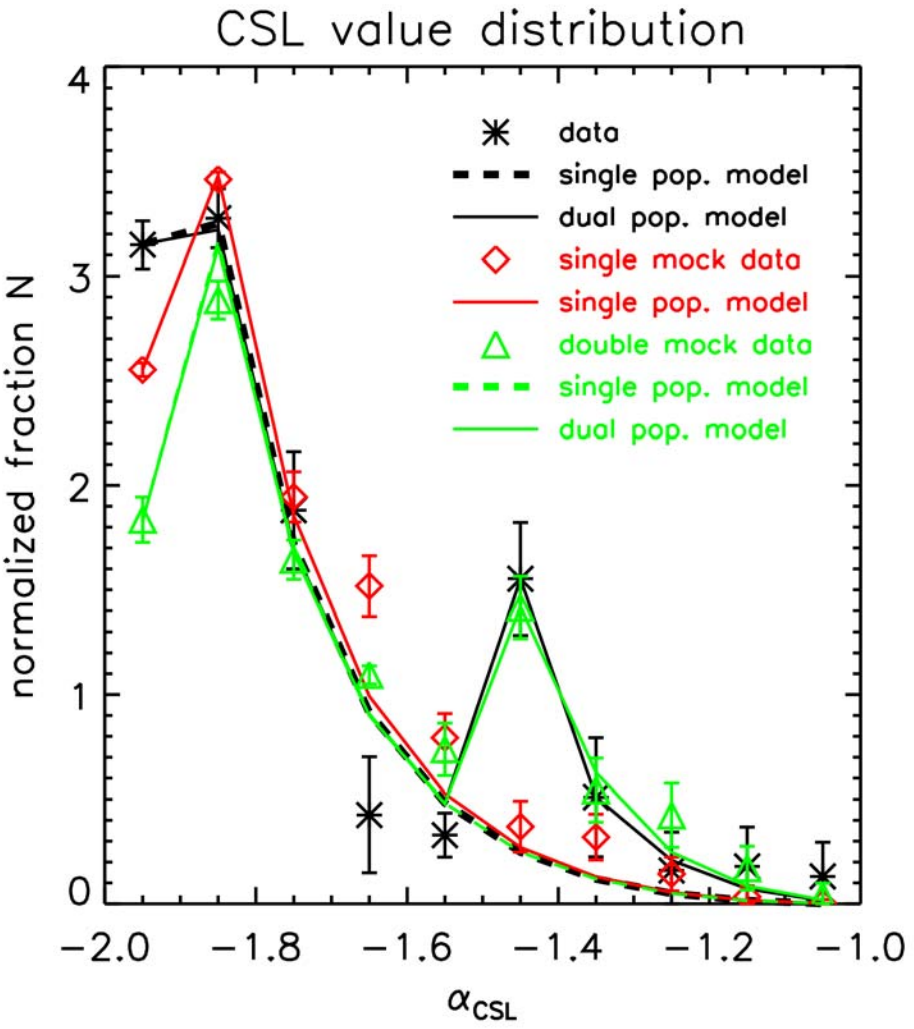

Fig. 2. Distribution of the CSL-limit values from our sample of 39 double image gravitational lenses (black asterisk symbols). The observations are overlaid with fitted distribution for single population (black dashed line) and dual population model (black solid line). Correspondingly, created 100 lens single population mock data is presented with red diamonds, and fit to the data with solid red line. Green triangles correspond to 100 lens system mock data containing two populations of halos ($\alpha_I = -1.96$, $P_I = 0.83$, $\alpha_{II} = -1.49$ and $P_{II} = 0.17$), and green dashed and green solid lines corresponding CSL-fits. The curves are renormalized to cover an unit area and P_I and P_{II} are occurrence probabilities.

5. Synthetic lens catalogue

Effects from the error sources on the distribution of the CSL values are studied by constructing mock lens catalogues. Although the CSL-limit of a lens system does not depend on the mass or the concentration of the lens nor the distances between the observer, the lens and the source, the created mock data should resemble the real lensing data as closely as possible. The distributions of the image separations, the lens redshifts, the source redshifts and the magnification ratios were compared between the generated mock-catalogue and the observed double image lenses. See figure 3.

The mock catalogue was created by sampling the Press-Schechter function at the suitable ranges for the masses and the redshifts for the lens and the source objects. The absolute luminosity of the source object is related to the sampled mass of the source [22]. The effects of the duty cycle time of the quasars on the luminosity function were ignored.

The magnification and the image separation biases were introduced by solving the lens equation (1) for the system including the perturbations from the error sources. The resulting lens system was accepted or rejected correspondingly if it exceeds the threshold magnitude and the necessary image separation for the detection. The K-correction nor the extinction need not to be accounted for, because our method uses flux ratios of the images.

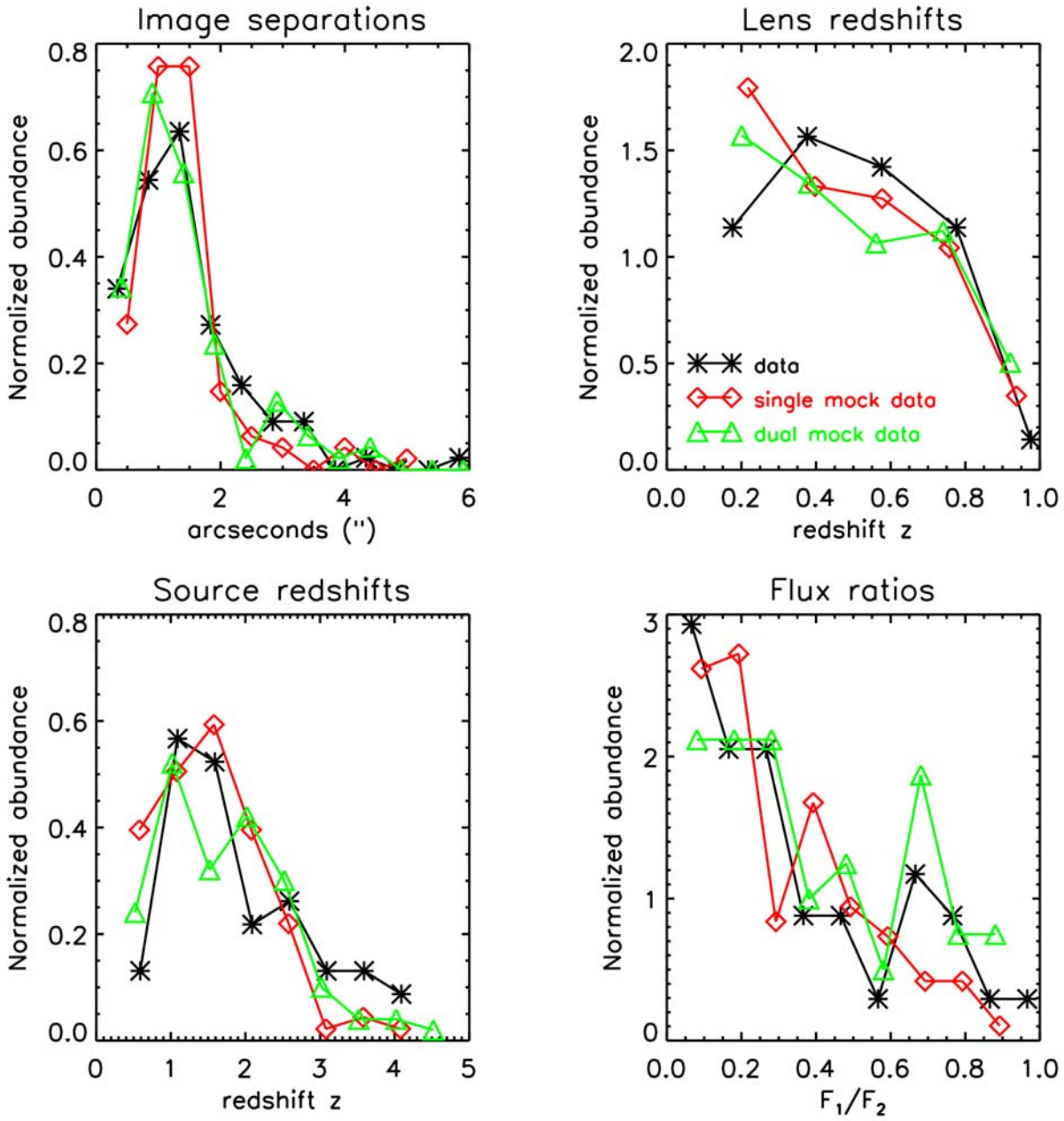

Fig. 3. Distribution of the image separations, the lens and the source redshifts and the flux ratios from observed data and the synthetic data created by sampling the Press-Schechter function (see caption for figure 2). The first set of the mock data (red) contains only one population of lenses with a universal cusp slope $\alpha = -1.95$. The second set of the mock data is created with two populations (green) with a universal cusp slopes $\alpha_I = -1.96$ and $\alpha_{II} = -1.49$. The corresponding probabilities for the lenses are $P_I = 0.83$ and $P_{II} = 0.17$. The curves are renormalized to cover an unit area.

The cosmological parameters $\Omega_m = 0.26$, $\Omega_\Lambda = 0.74$, $h = 0.7$ and $k = 0$ were used. The power spectrum normalization was $\sigma_8 = 1.07$ and the exponent $n = 0.95$. We generated a mock lens data, which resembles the observed data, see figure 3. The CSL-analysis recovers the universal cusp slope value from the same mock catalogue, as presented in figure 2. Recovered values are summarized in table 1.

6. Perturbations

In the final study, all the perturbing factors will be fully incorporated to the mock lens catalogue generation described in the previous section. Here we shortly summarize and analyze the contribution from each of the error sources. All the elements contributing to the observed magnification for each image in the lens system need not to be considered, because we are using flux ratios of the observed images. In our study we account the perturbations by the substructure within the lensing halos, the source variability through time

delay effects, the perturbations arising from the deviations from the axial symmetry and the microlensing.

	α_I	P_I	α_{II}	P_{II}
Data (single)	-1.95±0.06	1.0	-	-
Data (double)	-1.95±0.06	0.83	-1.45±0.2	0.17
Single mock data	-1.94±0.03	1.0	-	-
Double mock data (single)	-1.93±0.05	1.0	-	-
Double mock data (double)	-1.93±0.05	0.80	-1.46±0.14	0.20

Table 1. Fitted cusp slope values for the observational data, and the single and the double population mock data. The single population mock data was created with a universal cusp slope $\alpha = -1.95$ and the dual population model with the universal cusp slopes $\alpha_I = -1.96$ and $\alpha_{II} = -1.49$. The corresponding probabilities for the lenses are $P_I = 0.83$ and $P_{II} = 0.17$. Error limits are from the covariance matrix acquired from the Levenberg-Marquardt fitting method. The population probabilities are calculated from the normalizations provided by the fitting method.

According to the N-body simulation studies of the structure formation, the dark matter halos should possess significant amount of substructure in the form of subhalos [16]. Perturbations by the substructure in the lens halos are considered using the linearized theory as presented in [23]. The theory indicates that the brighter image is always brightened more than the dimmer image in a double image lens, thus the substructure always decreases the magnification ratios. This effect tends to shift the distribution presented in figure 2. towards $\alpha = -2$ (leftwards) and erase all the features with greater values.

The changes in the magnification by the substructure are roughly proportional to the square of the macrolens magnification. Thus the magnification ratio is affected the most nearby the critical curves of the lens and the effects become negligible elsewhere. Lensing near critical curves produce (partial) Einstein rings that are excluded from our data, because they are not seen as double image lenses. Furthermore, their relative abundance is small when sources are distributed uniformly on the source plane, because the source must lie close to the optical axis. The same argument can be applied to the microlensing by the stars within the lens galaxy. The realistic amounts of substructure in the lensing halo produce negligible effects on the CSL-distribution.

When the source image luminosity is fluctuating, the time delay between the images produced by the lens corrupts the flux ratio. The lens equation (1) can be used to derive the amount of time delay for each lens configuration. The intrinsic source variability connected to the time delay is modeled as a power law noise, which corresponds to the observed properties of the quasar variability [24]. The variability is scaled according to the modeled structure function and parametrization as presented in [25]. The magnitude of fluctuations is proportional to the time delay, which is usually order of few or few tens of days, depending on the geometry of the lensing. On average this corresponds roughly 0.2 magnitudes in the absolute magnitude of the source, although there are sources with more extreme variability. When it is converted to the fluxes and magnification ratios, it is roughly 0.9% of the baseline magnitude, that corresponds order of 2% in the magnification ratio. On average this large deviation should have negligible effects on the CSL-statistics.

In reality most lenses are not axially symmetric, but they have some degree of intrinsic ellipticity in their lensing potential and/or they are perturbed by an external lensing potential, i. e. other nearby galaxies. The critical curves of the elliptic and the sheared lenses are diamond shaped, and sources nearby the critical curves produce more than two images (usually four). Such lens systems are excluded from our sample as are lenses with strongly perturbing companions.

Elliptic halos produce also double image lenses, but the deviations from the axial symmetry are tolerable when lensing does not take place at the vicinity of the critical curves and ellipticities are reasonable. Additionally, when randomly oriented three dimensional lensing halos are projected to the lensing plane, an average amount of ellipticity in the projected lensing potential is somewhere between none and the maximum asymmetry of the triaxial halo. Thence ellipticities of the lens halos should produce only statistical noise in the CSL-statistics, that should be manageable.

Finally, we consider microlensing by stars in our galaxy. In principle a microlens event can significantly enhance already lensed image, corrupting the magnification ratio and the CSL-statistics. However, microlensing events are very rare, because they require very precise alignment. In the OGLE project, 20.5 million stars in the galactic bulge cloud were monitored during three year period, and 214 cases of microlensing were found [26]. The probability for a single star in the bulge to be microlensed during one year of monitoring, is about 10^{-5}. If we consider double image lens systems, which are not observed at the regions of high stellar density in the Milky Way, a probability for a microlensing event in our sample consisting of 40 double image lenses is extremely small.

We can summarize, that perturbations can be treated as a statistical noise in our method because it is

based on the statistics of an extremal values for the required cusp slope for each lens. This conclusion will be further ensured by our mock lens catalogues, that will incorporate all these effects in a realistic way.

7. Conclusions

Here we have outlined a statistical method for estimating a universal cusp slope within a sample of double image lenses and presented preliminary results. Our method is based on an axially symmetric lens model. Although the axially symmetric lens model can not reproduce all the features seen in individual lenses realistic way, it can be used in statistical methods. Our method is based on a statistics of an upper limit for a required cusp slope for producing observed flux ratios, if we assume axial symmetry. It should be emphasized that we are not attempting to model each lens system in a realistic way. Our case is further strengthened by a close match between distributions of the CSL-values from the observational data, the mock data and the theory.

Additionally, because we are limiting ourselves to a lensing occurring far away from the critical curves, lensing problem becomes “nice”; there are no extreme magnifications, and effects from the substructure and ellipticities become tolerable. Therefore the axially symmetric lensing model is moderately good approximation for fluxes, and the whole problem can be linearized.

Our method suggests two populations of lenses, with occurrence ratio 1/6. The major population (I) of lenses in our sample has a cusp slope $\alpha \approx -1.95$ and the minor population (II) density profile with slope $\alpha \approx -1.45$. Corresponding occurrence probabilities are $P_I = 0.83$ and $P_{II} = 0.17$. The mock data is further strengthening this interpretation.

N-body simulations by [27] studying galaxy formation with dark and baryonic matter components, indicate similar populations for halos. Their results suggest that the population I halo profiles are steepened significantly by the baryonic matter component, and population II halos are dominated by the dark matter with a poor baryonic matter contribution.

Our method can be developed further to include lensing near the critical curves, thus accounting Einstein rings and four image lenses. Additionally, contribution of the perturbing factors can be studied through our method. For example, allowing too large amount of substructure within the halos would destroy the second population signature from the CSL-distribution.

References

1. Mutka, P. T. and Mähönen, P. H. // MNRAS, 373,243 (2006).
2. Mutka, P. T. // manuscript in preparation (2008).
3. Ma C.-P. and Bertschinger, E. // ApJ, 612, 28 (2004).
4. Williams, L. L. R., Babul, A. and Dalcanton, J. J. // ApJ, 604, 18 (2004).
5. Springel V. et al. // Nature, 435, 629 (2005).
6. Navarro, J. F., Frenk, C. S. and White, S. D. M. // ApJ, 462, 563 (1996).
7. Navarro, J.F., Frenk, C. S. and White, S. D. M. // ApJ, 490, 493 (1997).
8. Zhao, H. S. // MNRAS, 278, 488 (1996).
9. Fukushike, T., Kawai, A. and Makino, J. // ApJ, 588, 574 (2004)
10. Ricotti, M. // MNRAS, 344, 1237 (2003).
11. Burkert, A. // ApJ, 447, L25 (1995).
12. Moore, B., Quinn, T., Governato, F., Stadel, J. and Lake, G. // MNRAS, 310, 1447 (1999).
13. Ghigna, S., Moore, B., Governato, F., Lake, G., Quinn, T. and Stadel, J. // ApJ, 544, 616 (2000).
14. Ma, C.-P. // ApJ, 584, L1 (2004).
15. Zhang, T.-J. // ApJ 602, L5 (2004).
16. Metcalf, R. B., Moustakas, L. A., Bunker, A. J. and Parry, I. R. // ApJ, 607, 43 (2004)
17. Cohn, J. D. and Kochaneck, C. S. // ApJ, 608, 25 (2004).
18. Sand, D. J., Treu, T., Smith, G. P. and Ellis, R. S. // ApJ, 604, 18 (2004).
19. Buote, D. A. and Lewis, A. D. // ApJ, 604, 116 (2004).
20. Phillips, P. M., et al. // MNRAS, 328, 1001 (2001).
21. Kochanek, C. S., Falco, E. E., Impey C., Lehar, J., McLeod, B, and Rix H.-W. // CASTLES website, see http://cfa-www.harvard.edu/castles
22. Wyithe, J. S. B. and Loeb, A. L. // ApJ, 581, 886 (2002).
23. Rozo, E., Zentner, A. R., Bertone, G. and Chen, J. // ApJ, 639, 573 (2006).
24. Timmer, J. and König, M. // A&A, 300, 707 (1995).
25. Vanden Berk, D. E. et al. // ApJ, 601, 692 (2004).
26. Udalski et al. // Acta Astron, 50, 1 (2000).
27. Gustafsson, M., Fairbairn, M., and Sommer-Larsen, J. // PRD, 74, 123522 (2006).